Mapping Individual Tree Species in an Urban Forest Using Airborne Lidar Data and Hyperspectral Imagery

AAG Remote Sensing Specialty Group 2011 Award Winner[1]

Caiyun Zhang and Fang Qiu

Abstract

We developed a neural network based approach to identify urban tree species at the individual tree level from lidar and hyperspectral imagery. This approach is capable of modeling the characteristics of multiple spectral signatures within each species using an internally unsupervised engine, and is able to catch spectral differences between species using an externally supervised system. To generate a species-level map for an urban forest with high spatial heterogeneity and species diversity, we conducted a treetop-based species identification. This can avoid the problems of double-sided illumination, shadow, and mixed pixels, encountered in the crown-based species classification. The study indicates lidar data in conjunction with hyperspectral imagery are not only capable of detecting individual trees and estimating their tree metrics, but also identifying their species types using the developed algorithm. The integration of these two data sources has great potential to take the place of traditional field surveys.

Introduction

Urban forests have many benefits such as saving energy, improving water management, reducing air pollution, and connecting urban residents with nature (McPherson, 2006). To maximize these benefits, an urban forest inventory is often needed for planning and management purposes. Basic information in an urban forest inventory includes the number of individual trees, their species, spatial distributions, and health conditions. Traditionally, this information is collected through field surveys that are costly, labor-intensive, and time-consuming. In addition, field surveys can only be performed in areas accessible to the surveyors; little or no data may be collected for private properties and other inaccessible areas. It is difficult, if not impossible, to inventory urban forests for a whole city through field surveys. Consequently, relatively little information is available about the urban forest in most cities, a major constraint for realizing their benefits.

Remote sensing has become an attractive alternative to field surveys in forest inventory because of its lower total cost, greater coverage, and more regular data collection cycle. Recent developments in remote sensing have allowed for the detection of the 3D structure of forests and the estimation of forest attributes using the Light Detection And Ranging (lidar) techniques. Lidar has the ability to "see" the ground through openings in canopies and to estimate tree metrics (Lim *et al.*, 2003; Hyyppä *et al.*, 2008; Ustin and Gamon, 2010; van Leeuwen and Nieuwenhuis, 2010). Early generation of lidar based on laser profiling technology have long been used for estimating forest attributes at the stand level (Hyyppä *et al.*, 2008). However, for an urban forest, detailed information at the individual tree level is usually required. This is because an urban forest is a mosaic of a large number of trees with different species, ages, and a high degree of spatial heterogeneity. Fortunately, current lidar systems, based on laser scanning technology, have an extremely high sampling rate and are capable of estimating forest attributes down to the individual tree level. The literature has indicated that lidar can now effectively detect individual trees and estimate single tree metrics, such as tree heights and crown shape and size (e.g., Hyyppä and Inkinen, 1999; Persson *et al.*, 2002; Brandtberg *et al.*, 2003; Popescu and Wynne, 2004; Falkowski *et al.*, 2006; Chen *et al.*, 2006; Koch *et al.*, 2006; Kwak *et al.*, 2007; Morsdorf *et al.*, 2004; Tiede *et al.*, 2005; Zhang, 2010; Li *et al.*, 2012). However, most lidar systems have only one or two bands. This is insufficient for tree species identification, especially in urban forests with diverse species and high spatial heterogeneity. Hyperspectral sensors, usually possessing hundreds of bands, exhibit a great potential in identifying tree species with their rich spectral contents.

A number of studies were conducted to classify tree species from hyperspectral imaging data with varying degrees of success (e.g., Martin *et al.*, 1998; Xiao *et al.*, 2004;

[1] In recognition of the 100th Anniversary of the Association of American Geographers (AAG) in 2004, the AAG Remote Sensing Specialty Group (RSSG) established a competition to recognize exemplary research scholarship in remote sensing by post-doctoral students and faculty in Geography and allied fields. Dr. Caiyun Zhang submitted this paper which was selected as the 2011 winner.

Caiyun Zhang is with the Department of Geosciences, Florida Atlantic University, 777 Glades Road, Florida 33431 (czhang3@fau.edu).

Fang Qiu is with the Program in Geospatial Information Sciences, University of Texas at Dallas, 800 West Campbell Road, GR31, Richardson, Texas 75080.

Photogrammetric Engineering & Remote Sensing
Vol. 78, No. 10, October 2012, pp. 1079–1087.

0099-1112/12/7810–1079/$3.00/0

Thenkabail *et al.*, 2004; Clark *et al.*, 2005; Buddenbaum *et al.*, 2005; Boschetti *et al.*, 2007), but their applications in urban forests are limited. This is because, unlike natural forests with uniform stand characteristics, trees in urban settings are often isolated single trees or clumped groups, with varying tree heights, crown widths, multiple treetops, and different degrees of canopy overlaps. This complexity has made characterizing urban trees difficult (Xiao *et al.*, 2004). Urban forests are also composed of a mixture of trees of diverse species, varying ages, and different health conditions. These factors combined result in a high degree of between-species spectral confusion and a great deal of within-species spectral variability. A noted remote sensing scientist, Dave Simonett, has said "Green is green is green" (Jensen, 2005). By this he meant that most trees will likely appear similar in their signatures throughout the spectrum. On the other hand, differences in age, health condition, or the amount of gaps presenting in tree crowns may cause the same species to appear spectrally different. When traditional pixel-based classifiers are used to differentiate the species, pixels of different species may be misclassified as the same types and pixels of the same tree may be classified as different types. This may result in a very noisy species classification map, especially in an urban forest with severe between-species spectral confusion and within-species variability problems. The noisy pixel-based species maps are not only full of errors, but also useless for community managers. Maps of individual trees with their corresponding species information are more desirable for urban forest management purpose.

Another challenge in urban tree species identification is the limitation of algorithms for hyperspectral data analysis. The traditional statistics-based multispectral image classifiers, such as the maximum likelihood approach, often fail to classify hyperspectral data due to the relatively small training samples compared to the high dimensionality of the hyperspectral data.

Endmember-based classifiers such as spectral angle mapper, linear spectral unmixing, and spectroscopic library matching, were thus specifically designed for hyperspectral data processing. These approaches may not achieve the expected results for identifying urban tree species due to the difficulties inherent in determining endmembers, the shortage of comprehensive spectral libraries of tree species, and the violation of the assumption in the algorithms that only one spectral representative (i.e., the endmember) exists for each species. Artificial intelligence techniques, such as fuzzy logic and neural networks, are another option. They have been extensively employed in multispectral image analysis (Mas and Flores, 2008), but their applications in hyperspectral image processing are still scarce. The employment of these techniques for urban tree species identification is even more limited. The main objective of this study is to develop an improved neuro-fuzzy system to identify tree species at the individual tree level from lidar and hyperspectral data. As a result, an individual tree based species map can be generated, which is more informative and useful than a traditional pixel-based species map.

Various studies have been conducted on the synergy of lidar and high spatial resolution multispectral images for forest inventory (Hyyppä *et al.*, 2008), but only a few studies have reported the integration of lidar with hyperspectral imagery for the purpose of urban forest inventory. Voss and Sugumaran (2008) fused hyperspectral imagery with several raster layers generated from lidar data to identify urban tree species using object-oriented image analysis techniques. Similarly, Dalponte *et al.* (2008) integrated lidar-generated rater layers with hyperspectral imagery to discriminate tree species on the pixel basis in a complex forest using support vector machine techniques. To the best of our knowledge, no efforts were made for mapping tree species at the individual tree level in complex urban environments with these two emerging data sources. In this study, we present a neuro-fuzzy approach to identify a large number of tree species in a complex urban forest down to the individual tree level. Single trees were first detected from lidar point cloud data, and then their species types were identified from the associated hyperspectral information. The potential to integrate lidar and hyperspectral imagery for urban forest inventory is also investigated. We hope this work will stimulate further research on the synergy of lidar and hyperspectral data and especially its applications in urban forests.

Methodology

Study Area and Data

The Turtle Creek in north Dallas, Texas was selected as the study area. The topography of the area is dominated by the Turtle Creek, which starts in north central Dallas (at 32°51' N, 96°48' W) and flows southwest five miles through Highland Park and University Park to its mouth on the Trinity River (at 32°48' N, 96°50' W). Elevation in the study area varies from 112 meters to 156 meters, with the lower elevations found over the creek and higher elevations observed along the bank of the creek. A false color composite in grayscale from the hyperspectral data is shown in Figure 1. This site is a typical urban area with complex spatial assemblages of vegetation, buildings, roads, creeks, and other man-made features. The area is dominated by broadleaved deciduous trees of different ages, with approximately 50 species found over the region. The broad range of tree species poses a challenge for current remote sensing-based forest inventory. The Turtle Creek area has a complex ecosystem and has been a center of interest and development in Dallas for over 100 years. To better manage this asset, help understand the current ecosystem, and encourage the development of priorities over this region, the Turtle Creek Association conducted a field survey in August 2008, which was followed by a simultaneous acquisition of small footprint, discrete-return lidar data and high spatial resolution hyperspectral images on 24 September 2008.

The field survey was conducted through a contract with Halff Associates, Inc. Only trees with a diameter at breast height (DBH) greater than four inches were measured and tagged with an identification number, resulting in a total of 2,602 trees being surveyed in the Turtle Creek Corridor. Tree location, species attributes, DBH, and health condition were recorded for each measured tree. Figure 1 shows the locations of these surveyed trees in white dots. More than 40 species were identified in the survey. The most common ten species are American Elm (*Ulmus americana*), Hackberry (*Celtis laevagata*), Pecan (*Carya illinoensis*), Eastern Red Cedar (*Carya illinoensis*), Shumard Red Oak (*Quercus shumardii*), Tree of Heaven (*Ailanthus altissima*), Cedar Elm (*Ulmus crassifolia*), Green Ash (*Fraxinus pennsylvanica*), Red Mulberry (*Morus rubra*) and Chinaberry (*Melia azedarach*).

Lidar data were collected by Terra Remote Sensing, Inc. (TRSI) using a proprietary Lightwave Model 110 whisk-broom scanning lidar system. The operation parameters in this mission are listed in Table 1. An average point density of 3.5p/m^2 was obtained due to an intentional 80 percent overlap between flights. The US Forest Service suggested a point density of ≥4 pts/m^2 for lidar application in forests (Laes *et al.*, 2008). The relatively lower density would not significantly influence its applications for deriving tree

Figure 1. A False Color Composite Image in Grayscale Derived from the Hyperspectral Data over the Study Area. Field Measured Trees Are Displayed in White Dots.

TABLE 1. OPERATION PARAMETERS FOR COLLECTING LIDAR AND HYPERSPECTRAL REMOTE SENSING DATA USED IN THIS STUDY (PROVIDED BY TERRA REMOTE SENSING, INC., 2008)

Aircraft Type	Piper Navajo
Flight Speed	235 km/hr (145 mile/hr)
Operation Altitude (m)	1260
Overlap (%)	80
Beam Divergence (mrad)	0.45
Scan Rate (Hz/Sec)	34
Laser Pulse Rate (kHz)	60
Returns	2
Laser Wavelength (nm)	1064
Scan Swath Width (m)	640
Off-nadir Scan Angle	26°
Footprint (cm)	93
Lidar Relative Accuracy (cm)	15
Lidar Absolute Accuracy (cm)	30

height and canopy size for this urban forest where most of trees are broadleaf with bigger canopies. The raw lidar point cloud data were processed by TRSI using Microstation™ Terrasolid and TRSI proprietary software. Final products were provided in the commonly used LAS lidar format with the projection of NAD_1983_UTM_Zone_14N.

Fine spatial resolution optical hyperspectral images were simultaneously acquired with the lidar data using an AISA Dual hyperspectral sensor. The AISA Dual sensor is a high performance, hyperspectral sensor system that concurrently collects both visible and near-infrared (VNIR) and shortwave infrared (SWIR) data. Hyperspectral images with 492 spectral bands were acquired at a spatial resolution of 1.6 meters. Radiometric calibration and geometric correction were performed by the vendor. The original images were transformed from raw digital numbers to radiance by applying a pixel-by-pixel correction using gain and offset. The offset was extracted from data stored in the "dark" files, which are sensor readings when the shutter is closed, representing sensor noise. The gain was extracted from the calibration files supplied by the sensor manufacturer. During the transformation from raw to radiance values further corrections for dropped lines and spectral shift were also applied. A transformation from radiance to surface reflectance of the entire image dataset was then carried out using ATCOR, a Modtran-based code specifically developed to perform atmospheric correction. For the geometric correction, the vendor used the lidar positional information to compute the real world coordinates of each pixel in the dataset to re-sample the hyperspectral images. The pre-processed images were then mosaiced and clipped for the study area.

Individual Tree Detection

In order to identify tree species at the individual tree level, single trees need to be detected first, which is primarily achieved from lidar data with two major steps (Zhang, 2010). The first step is the derivation of the Digital Terrain Model (DTM). Differences in height measurement caused by local terrain topography must first be eliminated in order to get the relative height of each lidar point. To this end, a DTM or Bare Earth Surface must be created and then subtracted from the original lidar hits. To generate the DTM, the lidar points reflected from the ground need to be filtered out from those reflected from above-ground objects. This process is known as "lidar data filtering" in the literature. Sithole and Vosselman (2004) compared eight filters and found that these filters perform well in smooth rural landscapes, but they all have poor performance in complex urban areas and rough terrain with vegetation. Since a variety of feature types (buildings, roads, trees, creeks, etc.) are present in our study area; none of those eight filters is likely to achieve satisfactory results for this area. Therefore, a vector-based filtering technique using a *k*-mutual nearest neighborhood clustering algorithm (Chang, 2011) was adopted. The idea of this algorithm is that points in a neighborhood sharing similar lidar attributes should belong to the same cluster which represents either ground or above-ground. A main advantage of this algorithm is that there is no loss of information by working directly with the raw lidar point cloud. Testing results illustrated that this approach had better performance in complex urban environments than commonly used raster-based lidar filters (Zhang, 2010).

The second major step is the detection of individual trees. This step includes treetop identification and tree crown delineation procedures. Several techniques have been explored in the literature to delineate tree crowns, detect treetops, and estimate single tree metrics. These approaches can be grouped into two categories: raster-based methods and vector-based

methods (Zhang, 2010). Raster-based methods segment individual trees from the lidar-derived canopy height model, a raster image interpolated from lidar points hitting on the surface of tree canopies. A major problem of those algorithms is the introduction of errors and uncertainties from the interpolation process (Smith *et al.*, 2004), which will ultimately affect the subsequent estimates of tree metrics (Suárez *et al.*, 2005). Vector-based methods detect trees and derive tree metrics using the original X, Y, Z or other attributes of the lidar point data without building a raster surface. We adopted the vector-based approaches developed in Zhang (2010) for individual tree segmentation because they may provide better accuracy by preserving the original elevation values.

To search for treetops in the above-ground lidar point cloud, which was derived by the lidar data filtering process, points hitting tree crowns need to be identified so that non-tree points will not interfere with individual tree isolation. The Normalized Difference Vegetation Index (NDVI) can be used for this purpose. We derived a NDVI image from the hyperspectral data and then spatially overlaid the above-ground lidar point cloud on it. The NDVI value at the cell within which the lidar point falls was then extracted as an additional attribute for the point. The vegetation points were then identified based on their NDVI values using a threshold.

To effectively and efficiently find treetops, the lidar points representing the surface of the tree canopy was first extracted by isolating them from the points that penetrate into the canopy. This step was accomplished by moving a square window over the study area in a non-overlapping manner and preserving the highest first-return pulse within it. After this, a treetop detection algorithm, referred to as a *tree climbing algorithm* was applied to identify the highest point (i.e., the treetop) of each individual tree. The idea of this algorithm is that the treetop always has the highest elevation and can be reached from a moving local window. After treetop detection, a tree crown delineation algorithm, referred to as the *donut expanding and sliding method*, was used to define tree crowns. This algorithm is the inverse process of the treetop finding procedure. A detailed description of individual tree segmentation, as well as a designed procedure for urban forest inventory (location, height, base height, crown depth, crown diameter, species) from lidar and hyperspectral imagery, were reported in Zhang (2010).

Tree Species Identification

Once individual trees and their tops are detected, their corresponding tree species need to be identified. We developed a neuro-fuzzy approach, referred to as *Adaptive Gaussian Fuzzy Learning Vector Quantization* (AGFLVQ), in order to effectively differentiate a large number of species using hyperspectral data, which is the focus of this paper. AGFLVQ is an improvement over Gaussian Fuzzy Learning Vector Quantization (GFLVQ) developed for hyperspectral image classification by Qiu (2008). One of the advantages of GFLVQ is its ability to perform supervised learning and unsupervised self-organizing simultaneously. The limitation of the GFLVQ is that it assumes each class has a same number of spectral representatives. This may lead to overestimation or underestimation of the number of clusters for some classes, thus will inevitably have negative impacts on the final classification accuracy. It is therefore necessary to improve the GFLVQ by exploring a fully adaptive neuron-fuzzy approach that can automatically determine the number of competitive neurons to characterize the degree of within-class spectral variability. To this end, the AGFLVQ is developed as follows.

An illustration of the topological structure of AGFLVQ with varied numbers of spectral clusters for each species in the competitive layer is displayed in Figure 2. The AGFLVQ has three layers: an input layer, a competitive layer, and an output layer. The neurons in the input layer correspond to the input pixel values of all the hyperspectral bands. The number of neurons in the output layer equals the number of species types. The number of neurons in the competitive layer can be equal to or greater than that of the output classes. When the number of competitive neurons is more than the number of classes, each class is allowed to have multiple clusters so that the modeling of possible multi-modal distributions in the data is possible. The AGFLVQ system can automatically adapt the number of neurons in the competitive layer based on a student t-test. Externally the AGFLVQ is a supervised neuro-fuzzy system, but internally, it has a fully unsupervised engine that can generate an appropriate number of competitive neurons for each output class, which makes it more robust than GFLVQ. The output and competitive layers are not fully connected, as shown in the illustration.

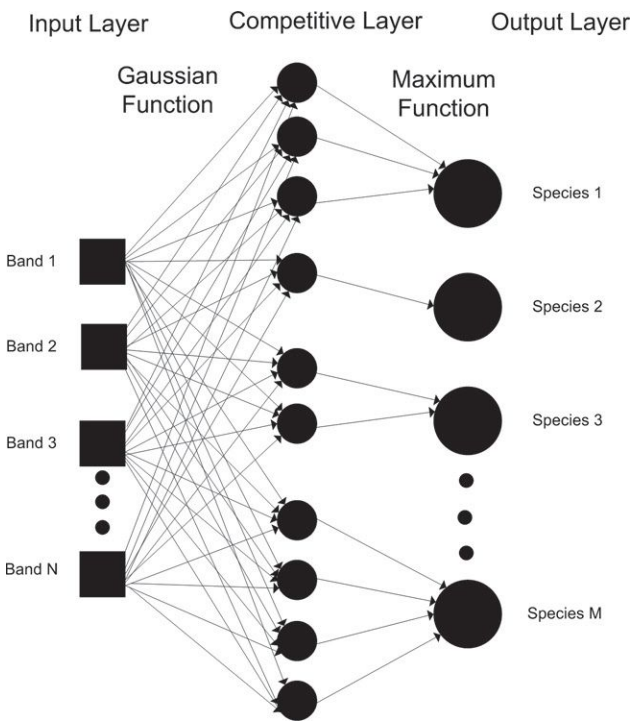

Figure 2. Topological Structure of the AGFLVQ System with Adaptive Clusters for Each Output Class.

The AGFLVQ approach contains the fundamental ingredients of both a neural network and a fuzzy system, and consists of the following components: (a) fuzzification and initialization, (b) generation of clusters, (c) neuro-fuzzy learning, and (d) neuro-fuzzy classification and defuzzification. Each component is described in detail below.

Fuzzification and Initialization

Since the inputs into the system are usually not fuzzy numbers, the training samples need to be fuzzified into a set of fuzzy numbers before entering the system. The fuzzification of a single input neuron is achieved by using the Gaussian fuzzy membership function:

$$A_{ij} = e^{-\frac{(c_{ij}-x_j)^2}{2\times\sigma_{ij}^2}} \quad (1)$$

where A_{ij} is the membership grade, c_{ij} is the mean parameter of the Gaussian function corresponding to the center of the

i^{th} cluster of the j^{th} input neuron, and x_j is the j^{th} input variable (that is, input pixel value for j^{th} band), and σ_{ij} represents the Gaussian standard deviation parameter characterizing the degree of dispersion of the cluster. Equation 1 can only be used to determine the fuzzy membership grade of a pixel for one band. For hyperspectral data, to assign a pixel to a particular cluster or class, the input values of all the bands of this pixel need to be considered. This is achieved using an *and-or* fuzzy operator in the form of the geometric mean so that an overall membership grade of this pixel can be obtained by:

$$\alpha_i = \left(\prod_{j=1}^{n} e^{-\frac{(c_{ij} - x_j)^2}{2 \times \sigma_{ij}}} \right)^{\frac{1}{n}} \quad (2)$$

where α_i refers to the overall membership grade of the input pixel concerning the i^{th} output cluster, n refers to the number of input neurons, and c, x, i, j, and σ are the same parameters as in Equation 1. This operator is an averaging operator; i.e., it allows a low membership grade in one band to be compensated for by a high membership grade in another band, so that a missing or noisy value in one band will not heavily affect the classification output of the entire pixel.

Two parameters (c and σ) need to be initialized before running the AGFLVQ algorithm. Instead of assigning random values for initialization like most neural networks applied to multispectral image classification, in AGFLVQ, these two parameters are initialized using the training data. AGFLVQ first randomly subdivides the training data for each species type into subsets according to the number of clusters configured for that species type. Then the mean and standard deviation of each subset are calculated and assigned to corresponding clusters as initial values for these two parameters. This training data informed initialization makes hyperspectral data classification more efficient (Qiu, 2008).

Generation of Clusters

The advantage of AGFLVQ over GFLVQ is the automatic generation of clusters for each output class instead of using a constant number. To automatically generate the number of clusters for each species, internally unsupervised fuzzy self-organizing map (Zhang and Qiu, 2011) clustering is performed first with a predetermined number of clusters (e.g., 5) for each species, then a two sample Student t-test is used to assess the similarity of the Gaussian distribution of two adjacent clusters. The two-sample student t-test can test the equality of two means from two groups with equal sample sizes and equal variance, or with unequal sample sizes and equal variance, or with unequal sample sizes and unequal variance. After the unsupervised clustering, clusters within each species should have different sample size and variance. Thus the two-sample t-test for unequal sample sizes and unequal variance was used with the equations as:

$$t = \frac{c_{ij} - c_{(i+1)j}}{S_{c_{ij} - c_{(i+1)j}}} \quad (3)$$

$$S_{c_{ij} - c(i+1)_j} = \sqrt{\frac{\sigma_{ij}^2}{n_1} + \frac{\sigma_{(i+1)_j}^2}{n_2}} \quad (4)$$

where c_{ij} and σ_{ij} are the same parameters as for Equation 1, and n_1 and n_2 are the total number of samples for cluster i and cluster $i+1$, respectively. A p value for each test can be calculated based on the t distribution. If the p value is greater than 0.05, indicating the two clusters are basically from the same distribution, then the two adjacent clusters are merged; otherwise, they are kept separated. The merging of the clusters can be conducted iteratively until no more merging is needed. In this way, the number of competitive neurons for each species can be finally determined automatically.

Neuro-fuzzy Learning

Two parameters (c_{ij} and σ_{ij}) are updated during the training process by using the externally supervised learning algorithm, which is, utilizing the true target species information provided by the training data. The updating schemes are:

$$\begin{cases} \Delta c_{ij} = \eta(x_j - c_{ij}) \\ \Delta \sigma_{ij} = \eta(|c_{ij} - x_j|) \text{ if } x \text{ and } c \text{ belong to the same species type} \end{cases} \quad (5)$$

$$\begin{cases} \Delta c_{ij} = 0 \\ \Delta \sigma_{ij} = 0 \text{ if } x \text{ and } c \text{ not belong to the same species type} \end{cases} \quad (6)$$

The supervised learning method for the mean parameter has the effect of moving the mean parameter c_{ij} (the cluster center) towards the matched (correctly classified) input pattern. Unlike GFLVQ that pushes c_{ij} away from the unmatched (incorrectly classified) input pattern, AGFLVQ uses only one learning scheme for the mean parameter because of the high degree of similarity of spectral characteristics between tree species types. The "pushing away" scheme may push the mean parameter far from the center of the cluster, resulting in unexpected relearning. The geometric interpretation of the updating rule for σ_{ij} is that when the absolute deviation of the input pattern x_j from the center of the matched cluster (centered at c_{ij}) is larger than the current standard deviation σ_{ij} of the cluster, the standard deviation will be increased by η portion of the difference. If the absolute deviation is smaller, then the standard deviation will be decreased by the smaller portion of the difference. This ensures the size of the cluster to be shrunk or enlarged adaptively based on the deviation of all the matched input patterns from the cluster center. If the input pattern x_j belongs to a different cluster, then no update is needed because the cluster has nothing to do with the input pattern, similar to the GFLVQ system.

Neuro-fuzzy Classification and Defuzzification

All the automatically generated clusters from the internally unsupervised clustering and externally supervised learning can be used to directly classify the data. Fuzzy membership grades are calculated for an input pixel first, and then defuzzification is performed by comparing all the membership grades of the pixel and then assigning the pixel to the class with the maximum membership grade.

Results and Discussion

The lidar algorithms adopted in this study for data filtering, individual tree detection and crown delineation generated good results (Zhang, 2010). An average agreement of 93.5 percent was obtained for the lidar tree detection algorithm by comparing the number of lidar detected trees with the number of field surveyed trees in the Turtle Creek Corridor. For the entire study area, a total of 20, 736 dominant trees were detected from the lidar data, whose species need to be identified.

A lidar-detected individual tree can be conceptualized as an object comprised of lidar points representing its tree crown, including the associated treetop. Therefore, the assignment of each individual tree to a specific species is achieved using object level tree species classification, rather than traditional pixel level classification. Object level species classification can be conducted by analyzing the

typical values of the hyperspectral pixels corresponding to all the points falling within a crown, referred to as crown-based species classification, similar to most object level classification approaches. Alternatively, species classification can also be achieved by analyzing only the hyperspectral pixel value corresponding to the treetop, known as treetop-based species classification.

The developed AGFLVQ method is capable of performing both crown-based and treetop-based species classification. However, crown-based species classification for individual trees has several disadvantages compared with treetop-based classification. First, a representative spectral signature for a crown is difficult to determine, because each tree crown often has an illuminated side and a shaded side. The spectra of these two sides can differ significantly. Additionally, shadows and canopy gaps within a crown may introduce the mixed pixel problem. Second, errors are unavoidable during the tree crown delineation process, which can be propagated into, and impact significantly, the subsequent crown-based species classification. Crown delineation commission errors may group crowns of different trees into one object and thus incorporate spectral signatures of different species into one crown. This will complicate the crown-based species classification. Crown delineation omission error may result in small crown objects, which may not be able to provide a sufficient number of pixel values to generate statistically reliable and typical spectral signatures for the crowns. Additionally, more severe mixing pixel problems can occur at the boundary of tree crowns due to the possible inclusion of the spectra of different neighboring tree species or of bare earth into a pixel at the edge of crowns.

Treetop-based species classification at the individual tree level, however, has the following advantages compared with the crown-based species classification. First, the treetops are less likely to suffer from the double-sided illumination problem described above, because the treetops are often the best illuminated portion of a tree crown. Located in the middle of a tree canopy, treetops also have the least amount of shadow, gaps, and bare earth interference compared to the rest of the crown, and are therefore less impacted by the mixed pixel problem. The errors in the crown delineation have no impact on the classification because only the treetops are used to represent the spectral signature of a tree for species classification. In addition, a treetop-based species identification can save substantial computation time because only one hyperspectral pixel is processed for each tree. When species classification is completed, the identified species type for the treetop pixel can be assigned to the entire tree crown as object level information. For these reasons, the treetop-based species classification was employed to identify the species type of each individual tree using the hyperspectral pixel values over the lidar-detected treetops.

To apply the AGFLVQ algorithm, the hyperspectral pixel values for the treetops of all field-surveyed trees were first extracted from the hyperspectral imagery as the reference data. Out of 46 species in total, only the 40 species that had more than two field samples were used by the AGFLVQ algorithm. The number of reference data for the selected 40 species is shown in Table 2. These reference data were randomly divided into two parts. One part was used as training data, and the other part was employed as testing data for accuracy assessment. Statistical t-tests were conducted only for the first 20 species, which have more than 30 field samples, and only one cluster was defined for the other 20 species because they have a relatively small number of field samples. After training, species identification for lidar-detected trees in the entire study area was conducted by classifying the hyperspectral pixels corresponding to each treetop. The final identified species could be mapped on the crown basis by extending the treetop-based result to the lidar-delineated crown, as shown in Plate 1. A high spatial heterogeneity of trees and diverse species over this area is clearly observed. The individual tree based species map using either the treetops or the crowns is easier to use to the community managers.

The accuracy of the AGFLVQ algorithm was assessed by the conventional error matrix approach on the individual tree basis. The total accuracy was also calculated from the number of correctly identified trees against the total number of trees. The Kappa statistics is believed to be a better representation of the general quality of classification because it removes the effects caused by the differences in sample size and also accounts for the off-diagonal elements in the

TABLE 2. ACCURACY GENERATED FROM THE AGFLVQ FOR EACH SPECIES

ID	Species	PA (%)	UA (%)	NRD	ID	Species	PA(%)	UA (%)	NRD
1	American Elm	39.39	82.11	398	21	Bois d'arc	91.67	100.00	24
2	Hackberry	47.89	77.12	379	22	Sycamore	72.73	80.00	21
3	Pecan	65.55	60.94	237	23	Black Locust	87.50	100.00	15
4	Eastern Red Cedar	62.93	73.00	232	24	Redbud	100.00	100.00	13
5	Shumard Red Oak	77.27	65.89	219	25	Persimmon	100.00	100.00	6
6	Tree of Heaven	76.36	47.19	220	26	Slash Pine	100.00	100.00	5
7	Cedar Elm	83.54	52.80	159	27	Gingko	100.00	100.00	5
8	Green Ash	87.23	65.08	94	28	Southern Magnolia	100.00	100.00	5
9	Red Mulberry	84.62	71.74	77	29	Dogwood	100.00	100.00	4
10	Chinaberry	78.79	68.42	65	30	White Ash	100.00	100.00	4
11	Gum Bumelia	88.89	85.71	54	31	Bradford Pear	100.00	100.00	3
12	Bald Cypress	84.00	77.78	49	32	Chinese Pistache	100.00	100.00	3
13	Cherry Laurel	95.00	59.38	39	33	Chinese Tallow	100.00	100.00	3
14	Boxelder	90.00	81.82	38	34	Southern Catalpa	100.00	100.00	3
15	Post Oak	100.00	86.36	38	35	Sweetgum	100.00	100.00	3
16	Live Oak	89.47	85.00	37	36	Golden Rain Tree	100.00	100.00	2
17	Bur Oak	94.12	80.00	34	37	Black Walnut	100.00	100.00	2
18	Cottonwood	94.12	94.12	34	38	Honey Locust	100.00	100.00	2
19	Crepe Myrtle	100.00	100%	32	39	Western Soapberry	100.00	100.00	2
20	Black Willow	93.75	88.24	31	40	Catalpa	66.67	100.00	2

Total Accuracy: 68.8% Kappa Value (k_hat): 0.66 Z-Score: 47.76
PA: Producer's Accuracy UA: User's Accuracy NRD: Number of Reference Data

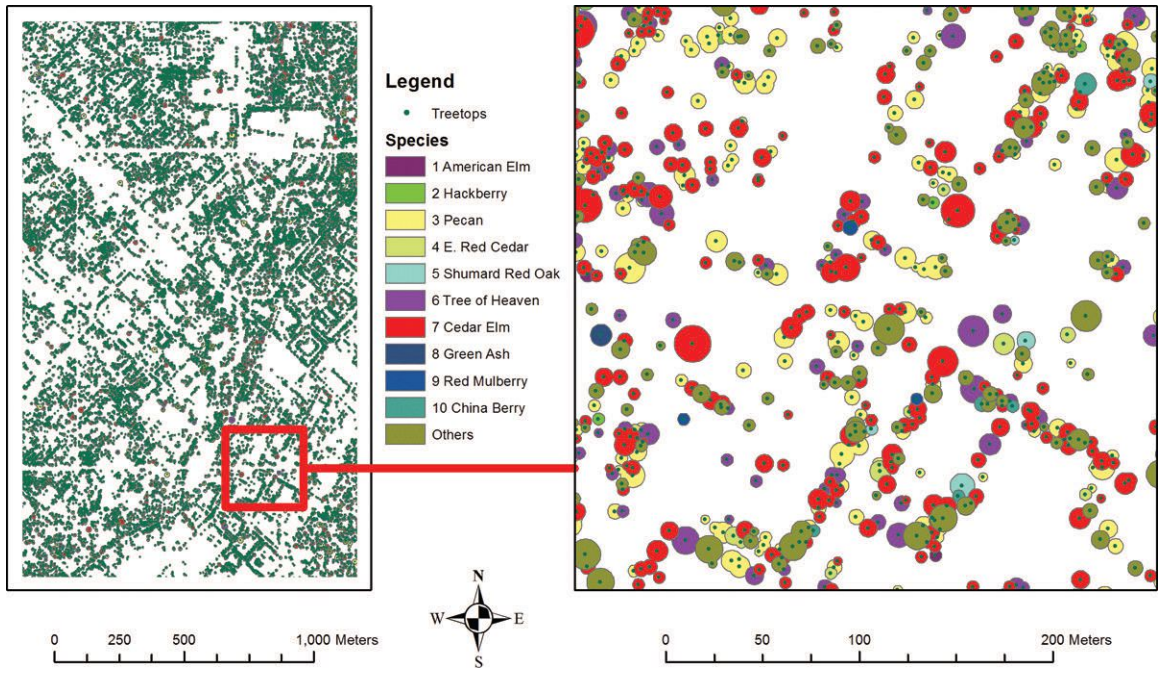

Plate 1. Species Map on the Crown Level with the Detected Treetops. The complexity of the urban forest with rich species, varying crown size, and high spatial heterogeneity, are presented.

error matrix (Congalton *et al.*, 1983). Thus, the Kappa value was also calculated to quantify the classification accuracy. After running the algorithm 100 times with different training and testing data selected, the average of the producer's and user's accuracy of each species, the average of the overall accuracy and Kappa statistics were calculated, which are given in Table 2. The producer's accuracy varies from 39.39 percent to 100 percent, and the user's accuracy ranges from 47.19 percent to 100 percent for different species. The most common species: American Elm, Hackberry, and Cedar Elm, all belong to the Elm family, resulting in a poor accuracy in classification due to their similarity in plant biochemistry. Good accuracy was achieved for the less common species. The overall averaged accuracy of classification is 68.8 percent, and the Kappa value is 0.66. These accuracy measures are more robust than those obtained by training and testing the algorithm with the same data group. To examine the significance of the result, the Kappa z-score statistical test based on the error matrix was conducted. The derived value of z-score is 47.76, suggesting the result is significantly better than a random classification at the 95 percent statistical confidence level. For comparative purposes, the traditional spectral angle mapper (SAM) method for hyperspectral data classification was also applied to identify tree species in the study region with the calculated mean spectrum as the endmember for each species. An overall accuracy of 39.95 percent and a Kappa value of 0.36 were obtained using the SAM method, illustrating that the AGFLVQ algorithm is more effective than the traditional SAM method.

It is difficult to compare the results obtained here with other studies using hyperspectral data for species identification due to differences in the study sites, the total number of species being discriminated, and the seasons in which data was collected. However, it is valuable to compare the results of other studies that were conducted under similar situations. In the literature, the work of Xiao *et al.* (2004) using AVIRIS imagery and the work of Voss and Sugumaran (2008) using lidar and hyperspectral imagery for urban tree species identification are most similar to this research. To provide a more legitimate basis for comparisons when different numbers of species are being identified, an index termed Number Of Categories Adjusted Index (NOCAI) is proposed. The NOCAI considers the number of tree species being differentiated and the accuracy of the obtained results. It is calculated by dividing the accuracy achieved by a specific algorithm by an expected accuracy that would be obtained if trees were randomly assigned to a species. The expected accuracy is simply $1/k \times 100\%$ where k is the number of species. Logically, the more the species, the lower the expected accuracy would be. Higher values for the NOCAI indicate better performance of the algorithm. Xiao *et al.* (2004) reported an average accuracy of 70% for identifying 12 deciduous tree species. The expected accuracy in Xiao *et al.* (2004)'s case is $(1/12) \times 100\%$, meaning an accuracy of 8.3% could be obtained by just randomly assigning a tree to a species type without using any classification methods. The NOCAI for the Xiao *et al.*' study is 8.4 (0.7/(1/12)). Voss and Sugumaran (2008) reported an overall accuracy of 57 percent for discriminating seven species; thus the value of NOCAI for their result is 3.99. In this study, an overall accuracy of 68.8 percent is achieved for identifying 40 species. An expected accuracy of 2.5 percent $((1/40) \times 100\%)$ could be obtained for a tree by just randomly assigning a tree to one of 40 species. The calculated value of the NOCAI is 27.52. This higher NOCAI value suggests that the developed approach is effective to discriminate a large number of tree species for an urban forest, based upon comparison with Xiao *et al.*(2004)'s multiple-masking techniques and Voss and Sugumaran (2008)'s object-based approach.

Species identification is challenging because of the rich diversity of species and the spatial heterogeneity of urban forests. The AGFLVQ algorithm was able to provide good

accuracies on most species and yielded acceptable total accuracy and Kappa statistics for discrimination of 40 species in the study site. The result is significantly better than the traditional SAM hyperspectral classifier. This can be attributed to its capability to model the multiple spectral signatures within each species through the built-in unsupervised engine, as well as its power to catch the differences in the spectral mean and standard deviation between species. The adaptability of the competitive layer in AGFLVQ is also helpful for the achieved results. The adoption of the original GFLVQ could not generate a satisfactory accuracy. The between-species spectral similarity problem, and the varying degree of within-species variability is primarily responsible for the unsatisfactory result. While some species (such as many evergreen trees) exhibit relative within-species spectral homogeneity that can be captured by only one spectral signature, other species (such as many deciduous trees) may need two or more spectral signatures to characterize their within-species variability. The GFLVQ is unable to model this situation due to the fact that it assumes all the species have the same number of spectral signatures (or spectral clusters). Better accuracy may possibly be achieved if lidar-derived variables such as height, crown base height, and proportion of returns can be combined into the algorithm, which needs to be examined in the future. It is also worth mentioning that the time of data collection could impact the species classification accuracy. It has been found that good results can be obtained if the images are collected in the spring, shortly after the flushing of leaves, or in autumn, after trees have turned color (Lillesand and Kiefer, 1994). The imagery in this study was collected in summer, and most of the trees appear green with similar spectral characteristics throughout the visible portion of the spectrum; however, the richness of the spectral contents in hyperspectral data combined with a fine spatial resolution still made tree species identifiable. Potentially, better results could be achieved if data were collected in spring or autumn.

Conclusions and Future Research

The contribution of this research is the development of algorithms for automatically inventorying urban forests from lidar point cloud data and hyperspectral imagery. The study illustrated that tree species can be estimated with a reasonable accuracy by the proposed AGFLVQ from hyperspectral data at the individual tree level. Hyperspectral data have a powerful capability for identifying species due to their rich spectral contents. Taking the lidar derived treetop locations, tree species could be recognized by analyzing the hyperspectral data associated with these locations. The generated vector-based species map allows the query of species information of each individual tree, which is more useful for forest management than the traditional pixel-based species map. Lacking the concept of object, pixel-based species classification and mapping may result in different species types being identified as the same individual tree. Lidar data in conjunction with hyperspectral imagery are not only capable of detecting individual trees and estimating their tree metrics, but also identifying their species types using the proposed algorithm.

Note that only a simple integration of lidar and hyperspectral data was explored in this study. An in-depth fusion of lidar and hyperspectral data may further improve the accuracy of individual tree delineation, metrics estimation and species classification. For example, the spectral information may be used to provide a better crown delineation by excluding lidar points with very different spectra at the edge of the tree. Tree species identification may also be improved by making use of the tree lidar point density and the derived tree metrics as ancillary information to the current spectral-only classification if properly utilized. This in-depth lidar and hyperspectral data fusion could eventually accelerate the transition of lidar and hyperspectral applications in their respective field from scientific interests to commercial operational implementations. This research has laid down a solid foundation for further research on individual tree based analysis for urban forest inventory. A complete fusion of the two data sources for forest applications is one of the major directions for future research.

The developed algorithm for tree species identification was only tested in one study area. Additional research is needed in areas with different species, forest compositions, and sensors in order to examine the robustness and extensibility of this technique. We hope that the promising results for individual tree level species mapping obtained in this study will stimulate further lidar and hyperspectral remote sensing research and applications in many other urban forests of the world.

Acknowledgments

This research was jointly supported by the Global Change Research Program of China under Project 2012CB955603, and the Natural Science Foundation of China under Project 41076115. The Dallas Urban Forest Advisory Committee provided the datasets for this study.

References

Boschetti, M., L. Boschetti., S. Oliveri, L. Casati, and I. Canova, 2007. Tree species mapping with airborne hyperspectral MIVIS data: The Ticino Park study case, *International Journal of Remote Sensing*, 28:1251–1261.

Brandtberg, T., T. Warner, R. Landenberger, and J. Mcgraw, 2003. Detection and analysis of individual leaf-off tree crowns in small footprint, high sampling density lidar data from the eastern deciduous forest in North America, *Remote Sensing of Environment*, 85:290–303.

Buddenbaum, H., M. Schlerf, and J. Hill, 2005. Classification of coniferous tree species and age classes using hyperspectral data and geostatistical methods, *International Journal of Remote Sensing*, 26:5453–5465.

Chang, J., 2011. *Segmentation-based Filtering and Object-based Feature Extraction from Airborne LiDAR data*, Ph.D. dissertation, University of Texas at Dallas, Dallas, Texas.

Chen, Q., D. Baldocchi, P. Gong, and M. Kelly, 2006. Isolating individual trees in a Savanna woodland using small footprint lidar data, *Photogrammetric Engineering & Remote Sensing*, 72(9):923–932.

Clark, M.L., D.A. Roberts, and D.B. Clark, 2005. Hyperspectral discrimination of tropical rain forest tree species at leaf to crown scales, *Remote Sensing Environment*, 96:375–398.

Congalton, R.G., R.G. Oldwald, and R.A. Mead, 1983. Assessing Landsat classification accuracy using discrete multivariate statistical technique, *Photogrammetric Engineering & Remote Sensing*, 49(12):1671–1678.

Dalponte, M., L. Bruzzone, and D. Gianelle, 2008. Fusion of hyperspectral and LiDAR remote sensing data for classification of complex forest areas, *IEEE Transactions on Geoscience and Remote Sensing*, 46:1416–1427.

Falkowski, M.J., A.M.S. Smith, A.T. Hudak, P.E. Gessler, L.A. Vierling, and N.L. Crookston, 2006. Automated estimation of individual conifer tree height and crown diameter via two-dimensional spatial wavelet analysis of lidar data, *Canadian Journal of Remote Sensing*, 32:153–161.

Hyyppä, J., and M. Inkinen, 1999. Detecting and estimating attributes for single trees using laser scanner, *Photogrammetric Journal of Finland*, 16:27–42.

Hyyppä, J., H. Hyyppä, D.Leckie, F.Gougeon, X. Yu, and M. Maltamo, 2008. Review of methods of small-footprint airborne laser scanning for extracting forest inventory data in boreal forests, *International Journal of Remote Sensing*, 29:1339–1366.

Jensen, J.R., 2005. *Introductory Digital Image Processing*, Third edition, Upper Saddle River, New Jersey, Prentice Hall.

Koch, B., U. Heyder, and H. Weinacher, 2006. Detection of individual tree crowns in airborne lidar data, *Photogrammetric Engineering & Remote Sensing*, 72(3):357–363.

Kwak, D., W. Lee, J. Lee, G.S. Biging, and P. Gong. 2007. Detection of individual trees and estimation of tree height using LiDAR data, *Journal of Forest Research*, 12:425–434.

Lillesand, T.M., and R.W. Kiefer, 1994. *Remote Sensing and Image interpretation*, Third edition, New York, Wiley, ISBN 0-471-57783-9.

Laes, D., S. Reutebuch, B. McGaughey, P. Maus, T. Mellin, C. Wilcox, J. Anhold, M. Finco, and K. Brewer, 2008. *Practical Lidar Acquisition Considerations for Forestry Applications*, RSAC-0111-BRIEF1, Salt Lake City, Utah, U.S. Department of Agriculture, Forest Service, Remote Sensing Applications Center, 7 p.

Li, W., Q. Guo, M.K. Jakubowski, and M. Kelly, 2012. A new method for segmenting individual trees from the lidar point cloud, *Photogrammetric Engineering & Remote Sensing*, 78(1):75-84.

Lim, K., P. Treitz, M. Wulder, B. St-Onge, and M. Flood, 2003. Lidar remote sensing of forest structure, *Progress in Physical Geography*, 27:88–106.

Mas, J.F., and J.J. Flores, 2008. The application of artificial neural networks to the analysis of remotely sensed data, *International Journal of Remote Sensing*, 29:3617–3663.

Martin, M.E., S.D. Newman, J.D. Aber, and R.G. Congalton, 1998. Determining forest species composition using high spectral resolution remote sensing data, *Remote Sensing of Environment*, 65:249-254.

McPherson, E.G., 2006. Urban forestry in North America, *Renewable Resources Journal*, 24:8–12.

Morsdorf, F., E. Meier, B. Kötz, K.I. Itten, M. Dobbertin, and B. Allgöwer, 2004. Lidar-based geometric reconstruction of boreal type forest stands at single tree level for forest and wildland fire management, *Remote Sensing Environment*, 92:353–362.

Persson, Å., J. Holmgren, and U. Söderman, 2002. Detecting and measuring individual trees using an airborne laser scanner, *Photogrammetric Engineering & Remote Sensing*, 68(9):925–932.

Popescu, S.C., and R.H. Wynne, 2004. Seeing the trees in the forest: Using lidar and multispectral data fusion with local filtering and variable window size for estimating tree height, *Photogrammetric Engineering & Remote Sensing*, 70(5):589–604.

Qiu, F., 2008. Neuro-fuzzy based analysis of hyperspectral imagery, *Photogrammetric Engineering & Remote Sen*sing, 74(12):1235–1247.

Sithole, G., and G. Vosselman, 2004. Experimental comparison of filter algorithms for bare-earth extraction from airborne laser scanning point clouds, *ISPRS Journal of Photogrammetry and Remote Sensing*, 59:85–101.

Smith, S.L., D.A. Holland, and P.A. Longley, 2004. The importance of understanding error in lidar elevation models, *Proceedings of the ISPRS Congress*, Istanbul, Turkey, 12-23 July.

Suárez, J.C., C. Ontiveros, S. Smith, and S. Snape, 2005. Use of airborne LiDAR and aerial photography in the estimation of individual tree heights in forestry, *Computers and Geosciences*, 31:253–262.

Tiede, D., G. Hochleitner, and T. Blaschke, 2005. A full GIS-based workflow for tree identification and tree crown delineation using laser scanning, *Proceedings of CMRT 05, International Archives of Photogrammetry and Remote Sensing* (U. Stilla, F. Rottensteiner, and S. Hinz, editors), XXXVI(Part 3/W24), Vienna, Austria, 29-30 August.

Thenkabail, P.S., E.A. Enclona, M.S. Ashton, C. Legg, and M.J. De Dieu, 2004. Hyperion, IKONOS, ALI, and ETM+ sensors in the study of African rainforests, *Remote Sensing of Environment,* 90:23–43.

Ustin, S., and J.A. Gamon, 2010. Remote sensing of plant functional types, *New Phytologist*, 186:795–816.

Voss, M., and R. Sugumaran, 2008. Seasonal effect on tree species classification in an urban environment using hyperspectral data, LiDAR, and an object-oriented approach, *Sensor*, 8:3020–3036.

van Leeuwen, M, and M. Nieuwenhuis, 2010. Retrieval of forest structural parameters using LiDAR remote sensing, *European Journal of Forest Research,* 129:749–770.

Xiao, Q., S.L. Ustin, and E.G. McPherson, 2004. Using AVIRIS data and multiple-masking techniques to map urban forest tree species, *International Journal of Remote Sensing*, 25:5637–5654.

Zhang, C., 2010. *Urban Forest Inventory Using Airborne LiDAR Data and Hyperspectral Imagery*, Ph.D. dissertation, University of Texas at Dallas, Dallas, Texas.

Zhang, C., and F. Qiu, 2012. Hyperspectral image classification using an unsupervised neuro-fuzzy system, *Journal of Applied Remote Sensing*, 6:063515.